UNSYS digital

International Journal of Robotics and Mechatronics

A Smart Ultrasonic Actuator with Multidegree of Freedom for Autonomous Vehicle Guidance Industrial Applications

Mahmoud Shafik, M. Elvis Ashu, and B. Nyathi

College of Engineering and Technology, University of Derby, Derby, United Kingdom

***Abstract*—**A piezoelectric ultrasonic actuator with multidegree of freedom for autonomous vehicle guidance industrial application is presented in this paper. The actuator is aiming to increase the visual spotlight angle of digital visual data capture transducer. It consists of three main parts, the stator, rotor and housing unit. The stator is a piezoelectric ring made from S42 piezoelectric ceramics material, bonded to three electrodes made from a material that has a close Characteristics to the S42. The rotor is a ball made from stainless steel materials.

The actuator working principles is based on creating micro elliptical motions of surface points, generated by superposition of longitudinal and bending vibration modes, of oscillating structures. Transferring this motion from flexible ring transducer through the three electrodes, to the attached rotor, create 3D motions. The actuator Design, structures, working principles and finite element analysis are discussed in this paper.

A prototype of the actuator was fabricated and its characteristics measured. Experimental tests showed the ability of the developed prototype to provide multidegree of freedom with typical speed of movement equal to 35 rpm, a resolution of less than 5 μm and maximum load of 3.5 N. These characteristics illustrated the potential of the developed smart actuator, to gear the spotlight angle of digital visual data capture transducers and possible improvement that such micro-actuator technology could bring to the autonomous vehicle guidance and machine vision industrial applications. Furthermore research are still undertaken to develop a universal control prototype, integrate the actuator with an infrared sensor, visual data capture digital transducers and obtain the trajectory of motion control algorithm.

***Keywords*—**Multidegree of freedom actuator, autonomous vehicle, machine vision, robot guidance, mechatronics.

I. Introduction

AUTONOMOUS vehicles and driverless cars are key development for future smart cities and villages across the world. As the human eyes is one of the most important organs of the human body. Our abilities and talents are greatly depending on our ability to see, recognize, and distinguish objects and to estimate distances. Most jobs depend on our ability of visual perception. As amazing as the human sense of vision may be, we must admit that today's autonomous and manufacture technologies more and more often broaden well beyond the limits of human visual capacities. This is where artificial machine vision, autonomous vehicle and robot guidance technology comes in. It is one of the constantly growing areas of research and development that dealing with processing and analyzing of visual digital data capture [1-3]. It Plays a key role in the development of autonomous systems and enables decision making for some of the industrial applications and manufacturing process.

The principal aim and objectives of this research is to develop technology that has the ability to perceive, reason, move with multidegree of freedom and learn from experiences, at lower cost. The research is particularly focus on developing of an actuation system that could provide 3D motions with multidegree of freedom, to overcome the visual data capture transducer spotlight focus angle (**Figure 1**) and enhance the machine vision system ability to perceive and move in 3D.

Investigation into the state of the art of emerging cutting edge actuators technology and possible approaches to develop a creative, sustainable and simple design structure that meets the 3D motions and machine vision requirements, at lower cost was a challenge. However with the potential characteristics, design optimization and working mechanism that piezoelectric ultrasonic actuator technology offers and that could bring to this area of applied research industrial applications. There is a strong believes that this technology will fulfill the requirements and this is where this research programme has started.

The piezoelectric Ultrasonic actuators (USM) working principles are based mainly on the perception of driving the rotor by a mechanical vibration force generated on the stator (Lead Zirconate Titanate (PZT) Transducer), via piezoelectric inverse phenomenon. USM technology can be classified into many categories however the two main common categories, that based on the PZT working mode are, bonded type [5-9] and bolt-clamped type actuators [10-12]. USM's have many advantages and disadvantageous. These advantages are included compact size, high force density, and simple mechanical structure, slow speed without additional gear or spindle, high torque, non-magnetic operation, freedom for

Corresponding author: Mahmoud Shafik (e-mail: m.shafik@derby.ac.uk).
This paper was submitted on December 4, 2015; revised on December 20, 2015; and accepted on December 27, 2015.

constructional design, very low inertia, fast dynamic time responses, direct drive, fine position resolution, miniaturization and noiseless operation. These criteria gave them the potential to be used in a number of industrial applications [13-25]. Demanding and careful examination for piezoelectric ultrasonic actuators industrial applications reveals that there are apparent teething issues or disadvantageous. The first is in regard to its dynamic time response and transfer function. While a piezo-ceramic elements, typically PZT, expands in direct proportion to the magnitude of the applied voltage, the USM on the other hand accumulates those displacements over time. Therefore the transfer function of the actuator, relating to the magnitude of the driving signal to the displacement is an integrator [18, 21-26] and this showed a delay in the dynamic time response of the USM, but it is not nearly significant as that in an electromagnetic actuators i.e. DC and or AC. The second issue is that because motion is generated through a friction force between actuator elements therefore it has a dead band. Often USM does not move until the driving input signal is greater than 10% of the maximum allowed voltage, to overcome the friction, such a dead band limits the ability of USM to accelerate quickly [5, 21-26].

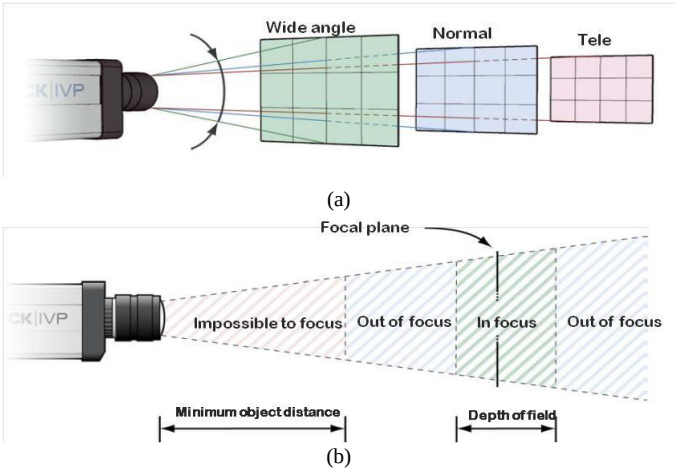

Figure 1 The camera (a) field of view in 2D showing the wide, normal and tele angle, (b) depth of field and minimum object distance [4]

The development of the proposed piezoelectric actuator with multidegree of freedom presented in this paper have passed through three main phases, phase one focused on: an investigation into the current actuators technology, phase two concentrated on: the actuator design and structure, phase three dealt with: finite element analysis, to test the actuator design structure, optimization and material micro deformation. The final stage focused on material selection, prototype fabrication, test and measurements.

II. USM WITH MULTIDEGREE OF FREEDOM AND STRUCTURE

Figure 2(a) and **(b)** shows the actuator design, structure and CAD sold model. **Figure 3** shows side view cross section of the actuator structure. The proposed actuator consists of three main parts, the rotor, stator and housing unit. The stator is a piezoelectric transducer ring made of Lead Zirconate Titanate - S42 piezoelectric material. Three titanium rods and a magnet were designed and attached to the stator, to support the rotor at three tips. The three rods has been detached at 120 degree and located at the transducer driving tips, to transfer the micro elliptical motion to the rotor. The rotor is a sphere of steel of size 28mm that rests on the stator intersecting at the tips of the rods. The structure is housed by Perspex, a transparent thermoplastic material.

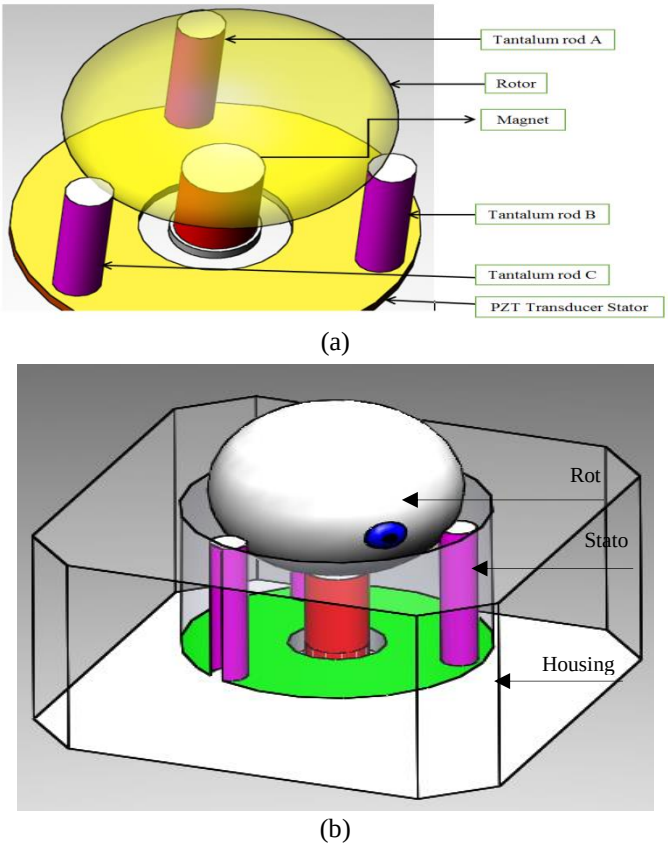

Figure 2 Design and structure of the proposed 3D USM for machine vision industrial applications: (a) design & structure, and (b) CAD solid model

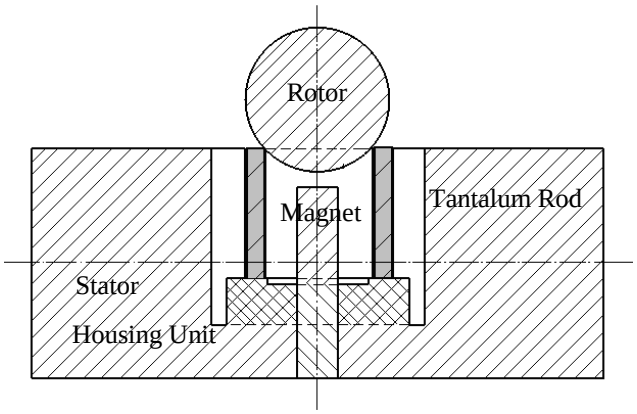

Figure 3 Cross section side view of the proposed 3D USM for machine vision and robot guidance industrial applications

The shape of three titanium rods is circular. This is to make sure that each rod is intersected with the sphere rotor in one single point. This is to minimize the friction force and avoid any possible loss of the stator thrust driving force. The three rods are fastened to the ring and the transducer ring is bonded to the housing using silicon rubber. This is to avoid any interference with the stator modes of vibration and provide the necessary degree of freedom, to transfer the micro elliptical force from the PZT ring to the rotor, through the three titanium rods. The magnet was design and its force has been determined carefully to keep the rotor attached to the rods and ensure efficient transfer of the stator vibration force.

The proposed actuator design in this paper has many advantageous over any other recently developed multidegree of freedom actuator. It presents a very creative, sustainable and simple design that is easy to manufacturer and maintained. The principles of motion is based on material deformation and friction force, therefore there is no much risk of interference and influences by any other system in the same working environment. This is in addition to the parts can be replaced if its performance deteriorated with the time as a very good example of sustainable innovation design approach. The design structure and working mechanism also presents for the first time a new approach that allows transferring the piezoelectric phenomenon through a material that has close characteristics (titanium materials) and performing the same principals of creating motion using friction between sold parts.

III. USM WITH MULTIDEGREE OF FREEDOM WORKING PRINCIPLES AND MATHEMATICAL MODEL

The proposed actuator is designed using bending and longitudinal vibration modes in a single ring transducer, which has a fixed wavelength. The concept is to utilize two modes of vibrations, to obtain the desired motion of the piezoelectric element, bending and longitudinal vibration modes. One mode of vibration produces a normal force while the other vibration generates thrust force, which is perpendicular to the normal force, resulting in an elliptical trajectory of micro elliptical motions, at a number of the rig surface tips.

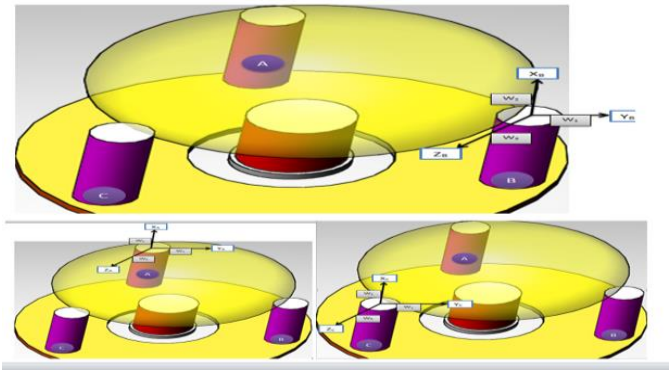

Figure 4 USM actuator showing the arragement of the rods A, B, and C on the piezoelectric flexural ring

The longitudinal and bending vibration modes are coupled by asymmetry of the piezoelectric ceramic vibration ring [8, 18-24]. By attaching three perpendicular rods A, B and C, with 120^{o} separation angle, to the piezoelectric ceramic ring surface, the micro elliptical motions are transferred to the rods tips, causing the rotor to move in 3D. The rotor movement is caused by the sequential frictional force generated at the tips of each rod. Obtaining the trajectory of these points across the sphere rotor will help to control the actuator movements. **Figure 4** shows the arrangement of the three rods and the sphere rotor of the actuator.

The following Equations (1), (2) and (3), represent the vibrations of the displacement in the parallel and perpendicular direction of the travelling wave generated by the flexural vibration ring transducer that transferred through the three rods, respectively.

$$X_A = W_1 \cos(2\pi f\ t + \alpha_1)$$

$$Y_A = W_2 \cos(2\pi f t + \alpha_2)$$

$$Z_A = W_3 \cos(2\pi f t + \alpha_3)$$

where: X_A, Y_A, and Z_A are the possible displacements in parallel and perpendicular direction, respectively. W_1, W_2, and W_3 are the maximum vibration amplitudes in the X, Y and Z directions, respectively. f is the resonant frequency, t is the time and α is the phase difference.

Obtaining and investigating the dynamic and mathematical model of the design structure could help to optimize the design and improve the performance of transferring the piezoelectric ring material deformation.

Figure 5 shows the coordinate system of the titanium rod A as the piezoelectric flexural ring start to vibrate.

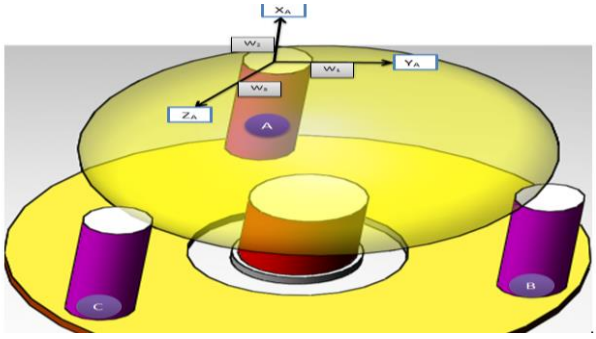

Figure 5 showing the coordinate of the titanium rod A attached to the piezoelectric flexural transducer ring

The piezoelectric actuator stator is a ring transducer and its model is the main principles to ensure the development of accurate results (Lizhong Xu & Shanjie Du 2013). According to Lizhong and Shanjie, the dynamic equation of the vibrating transducer (stator) as per figure above is given as:

$$\frac{\partial^2 w_1}{\partial \alpha^2} + \frac{1-\mu}{2}\frac{\partial^2 w_1}{r^2 \partial \varphi^2} + \frac{1+\mu}{2}\frac{\partial^2 w_3}{r \partial \alpha \partial \varphi} + \mu \frac{\partial w_2}{r \partial \alpha} = \frac{\rho h}{k}\frac{\partial^2 w_1}{\partial \tau^2}$$

$$\frac{1+\mu}{2}\frac{\partial^2 w_1}{r \partial \alpha \partial \varphi} + \frac{1-\mu}{2}\frac{\partial^2 w_3}{\partial \alpha^2} + \frac{\partial^2 w_3}{r^2 \partial \varphi^2} + \frac{\partial w_2}{r^2 \partial \varphi} = \frac{\rho h}{k}\frac{\partial^2 w_3}{\partial \tau^2} \quad (1)$$

$$\frac{12}{h^2}\left(\mu \frac{\partial w_1}{r \partial \alpha} + \frac{\partial w_3}{r^2 \partial \varphi} + \frac{w_2}{r^2}\right) + \nabla^2 \nabla^2 w = \frac{1}{D}\left(-\rho h \frac{\partial^2 w_2}{\partial \tau^2}\right)$$

where $w_1, w_2\ and\ w_3$ Are the axial, radial and tangential displacements of the vibrating transducer, respectively. The constants K and D could by obtained using:

$$K = \frac{Eh}{1-\mu^2}$$

$$D = \frac{Eh^3}{12(1-\mu^2)}$$

where μ is the Poisson's ratio for the transducer material, E is the elastic ratio of the vibrator transducer material, τ is the time, h is the thickness of the transducer disc, r is the radius of the transducer ring and ρ is the density of the transducer ring material.

According to lizhong and Shanjie in any circumferential mode n, the is a general relationship of a displacement for a free vibration mode and could be represented as:

$$w_1(\alpha,\varphi,\tau) = w_1(\alpha)\cos(n\varphi).e^{jw\tau}$$

$$w_3(\alpha,\varphi,\tau) = w_3(\alpha)\sin(n\varphi).e^{jw\tau} \quad (2)$$

$$w_2(\alpha,\varphi,\tau) = w_2(\alpha)\cos(n\varphi).e^{jw\tau}$$

where $w_1(\alpha), w_3(\alpha)\ and\ w_2(\alpha)$ Are correspond to the axial, radial and tangential displacement of the transducer respectively in the X_A, Z_A and Y_A direction of the electrodes A in the actuation system. **Figure 6** shows the displacement forces with a radius (r).

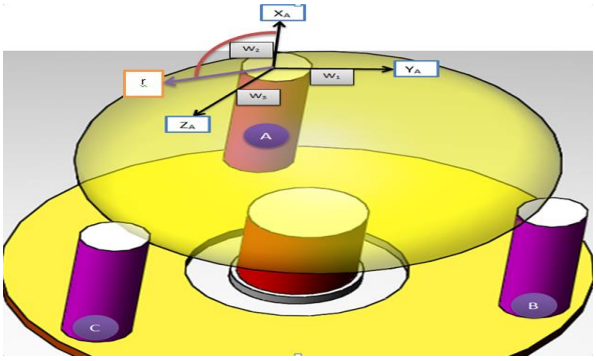

Figure 6 with estimated radial and the angle of rotation at electrode A of the actuation system (stator)

Substituting the displacement relationships into the dynamic equation and carry solving the differential equation will result to;

$$w_1''r^2 + \left[\Omega^2 - \frac{n^2(1-\mu)}{2}\right]w_1 + \frac{nr(1+\mu)}{2}w_3' + \mu r w_2' = 0$$

$$\frac{nr(1+\mu)}{2}w_1' - \frac{r^2(1-\mu)}{2}w_3'' + (n^2-\Omega^2)w_3 + nw_2 = 0 \quad (3)$$

$$\mu r w_1' + nw_3 + Kr^4 w_2{}^4 - 2Kn^2 r^2 w_2'' + [1 + Kn^4 - \Omega^2]w_2 = 0$$

where $\Omega^2 = \frac{\rho h r^2}{K}\omega^2\ and\ K = \frac{h^2}{12r^2}$

According to Lizhong and Shanjie the modal function can be describe along the axial direction can be described by a sum of linear combination of Fourier series that are orthogonal. The Fourier series in the axial, radial and tangential coordinates of the piezoelectric transducer disc motor can be express as:

$$w_1(\alpha) = A_{on} + \sum_{m=1}^{\infty} A_{mn}\cos\frac{m\pi\alpha}{l} \quad (0 \le \alpha \le l) \quad (4)$$

$$w_3(\alpha) = \sum_{m=1}^{\infty} B_{mn}\ \sin\frac{m\pi\alpha}{l} \quad (0 \le \alpha \le l) \quad (5)$$

With phases limit ranges with length l from:

$$lim \to -\left(\frac{\pi}{2}\right)w_0\ with\ (\alpha = 0)\ and\ \left(\frac{\pi}{2}\right)w_l\ with\ (\alpha = l)$$

$$w_2(\alpha) = \sum_{m=1}^{\infty} C_{mn}\ sin\frac{m\pi\alpha}{l}\ (0 \le \alpha \le l) \quad (6)$$

Relative derivatives of the above modal functions can be obtained to form the matrix in the form of:

$$\begin{bmatrix} D_1 \\ D_2 \\ D_3 \end{bmatrix} = \epsilon_0 \begin{bmatrix} E_1 \\ E_2 \\ E_3 \end{bmatrix}\begin{bmatrix} P_1 \\ P_2 \\ P_3 \end{bmatrix}, \quad \nabla.D = 0 \quad (7)$$

where D is the electric displacement, ϵ_0 is the vacuum permittivity, E is the electric field and P is the polarization density. The relative derivative of the modal functions, $w_1, w_3\ and\ w_2$ in the axial, radial and tangential direction is given as

$$w_1'(\alpha) = \begin{matrix} -((\pi^2)/2l)w_{01} \\ ((\pi^2)/2l)w_{l1} \end{matrix}\left[-\frac{\pi}{l}\sum_{m=1}^{\infty} mA_{mn}\ cos\frac{m\pi\alpha}{l} \quad (0 \le \alpha \le l)\right. \quad (8)$$

$$w_3'(\alpha) = \frac{\pi}{l}\left\{\frac{w_{30}+w_{3l}}{2} + \sum_{m=1}^{\infty}[w_{30} + V_{3l}(-1)^m + mB_{mn}]\cos\frac{m\pi\alpha}{l}\right\}\ (0 \le \alpha \le l) \quad (9)$$

$$w_2'(\alpha) = \frac{\pi}{l}\left\{\frac{w_{20}+w_{2l}}{2} + \sum_{m=1}^{\infty}[w_{20} + w_{2l}(-1)^m + mC_{mn}]\cos\frac{m\pi\alpha}{l}\right\}\ (0 \le \alpha \le l) \quad (10)$$

$$w_1''(\alpha) = \left(\frac{\pi}{l}\right)^2\ \left[\frac{w_{10}+w_{1l}}{2} + \sum_{m=1}^{\infty}[w_{101} + w_{1l1}(-1)^m - m^2A_{mn}]\ \ \cos\frac{m\pi\alpha}{l}\ (0 \le \alpha \le l)\right. \quad (11)$$

$$w_3''(\alpha) = \left(\frac{\pi}{l}\right)^{2} \begin{matrix} -((\pi^3)/2l^2)w_{302} \\ ((\pi^3)/2l^2)w_{3l2} \end{matrix} \left[\left\{ \sum_{m=1}^{\infty} [w_{30}m + V_{3l}m(-1)^m + m^2 B_{mn}] \sin\frac{m\pi\alpha}{l} \right\} \quad (0 \le \alpha \le l \right. \tag{12}$$

$$w_2''(\alpha) = \left(\frac{\pi}{l}\right)^{2} \begin{matrix} -((\pi^3)/2l^2)w_{202} \\ ((\pi^3)/2l^2)w_{2l2} \end{matrix} \left[\left\{ \sum_{m=1}^{\infty} [w_{20}m + V_{2l}m(-1)^m + m^2 C_{mn}] \sin\frac{m\pi\alpha}{l} \right\} \quad (0 \le \alpha \le l \right. \tag{13}$$

$$w_2'''(\alpha) = \left(\frac{\pi}{l}\right)^{3} \left\{ \frac{w_{202}+w_{2l2}}{2} + \sum_{m=1}^{\infty} [w_{202} + w_{2l2}(-1)^m - w_{20}m^2 - w_{2l}m^2(-1) - m^3 C_{mn}] \cos\frac{m\pi\alpha}{l} \right\} \quad (0 \le \alpha \le l) \tag{14}$$

$$w_2{}^4(\alpha) = \begin{Bmatrix} w_{204} \\ w_{2l4} \end{Bmatrix} \left(\frac{\pi}{l}\right)^{4} \sum_{m=1}^{\infty} [-w_{202}m - w_{2l2}(-1)^m + w_{20}m^3 + w_{2l}m^3(-1) + m^4 C_{mn}] \sin\frac{m\pi\alpha}{l} \quad (0 \le \alpha \le l) \tag{15}$$

Substituting Equations 4-15 into Equation 3 to obtain the form of Equation 7 for piezoelectric phenomenon yield for electrode A, B and C.

As per Lizhong and Shanjie the constants in Equation 16 above are given as

$$a_1 = \frac{n^2(1-\mu)}{2}, a_2 = \left(\frac{\pi r}{l}\right)^2, a_3 = \frac{\pi r}{l}\cdot\frac{n(1+\mu)}{2}, a_4 = \frac{\mu\pi r}{l}, a_5 = \frac{\mu-1}{2}a_2, a_6 = ka_2^2,$$

$$a_7 = 2kn^2 a_2, t_{11} = (n^2 - s_{22}s_{33})/\Delta_{mn}, t_{12} = m(a_4 n - a_3 s_{33})/\Delta_{mn},$$

$$t_{13} = m(a_3 n - a_4 s_{22})/\Delta_{mn}, t_{22} = (a_4^2 m^2 - s_{11}s_{33})/\Delta_{mn},$$

$$t_{23} = (ns_{11} - a_3 a_4 m^2)/\Delta_{mn}, t_{33} = (a_3^2 m^2 - s_{11}s_{22})/\Delta_{mn}, s_{11} = m^2 a_2 + a_1 - \Omega^2,$$

$$s_{22} = \frac{1-\mu}{2}a_2 m^2 + n^2 - \Omega^2, s_{33} = ka_2^2 m^4 + 2kn^2 a_2 m^2 + 1 + kn^4 - \Omega^2,$$

$$\Delta_{mn} = \begin{vmatrix} s_{11} & -a_3 m & -a_4 m \\ -a_3 m & s_{22} & n \\ -a_4 m & n & s_{33} \end{vmatrix}.$$

Equation 16 shows the dynamic equation of the actuation system with a transfer function represented in a piezoelectric matrix form which is the desire dynamics of the system.

IV. 3D USM Finite Element Analysis and Modelling

There are two methods of analysis can be used to model such USM's [6, 8, 10, 16-17, 24] since they have a number of complex non-linear characteristics. These methods are: the Analytical Analysis and the Finite Element Analysis (FEA) methods. FEA has been used in the design and development process lifecycle of this proposed actuator design. This is mainly aiming to evaluate the actuator structure, by performing an algebraic solution of a set of equations that describing an ideal model structure, with a finite number of variables. Some samples of the data used in the proposed actuator modelling are illustrated in **Tables I** and **II**.

The solid structure is divided into small portions named finite elements, an approximate solution for each finite element is generated. A summation of all the approximate solutions of the finite elements is obtained. The ring has been defined as made of piezoelectric Ceramic PZT-S42 material and the three rods have been selected as made of titanium material. ANSYS FEA CAD simulation software tools have been used in this analysis and simulation.

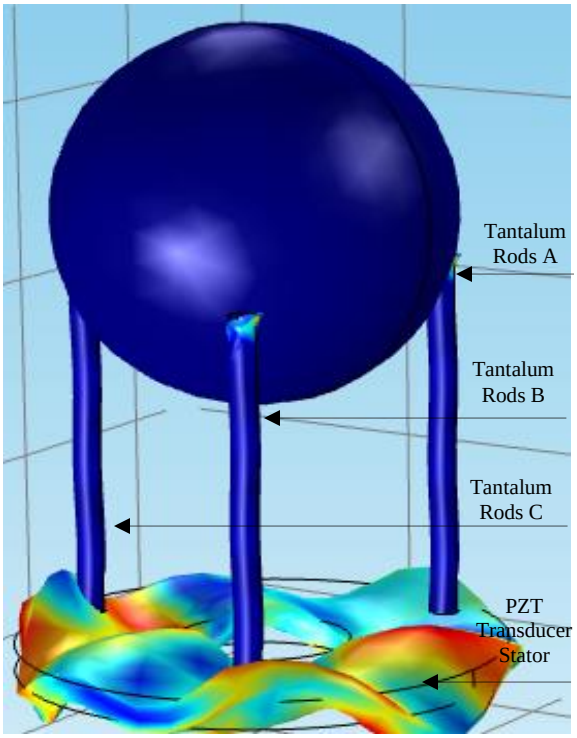

Figure 7 Actuator stator and rotor arrangements and principles used to generate 3D motions

As stated in **Table II**, the piezoelectric charge constant D_{31} rated as -155 is the working mode of the piezoelectric ring used to excite the bending vibrations of the ring. The D_{31} mode has a lower electromagnetic coupling efficiency compared to the D_{33} (320). The design dimensions of the stator for such actuator are mainly based on the vibration modes, capacitance ratio, and direction of vibratory displacement obtained using FEA [21, 22, 29-30]. **Figure 8** shows the FEA variations of the displacement of the PZT Transducer ring versus the exciting frequency, for the proposed USM actuator structure. This shows the natural frequency of the proposed structure is close to 40 kHz. It also shows the possible displacement and vibration amplitude that can be generated in the three dimensions due to the material deformation. The graph also evident that with any of the variable voltage or frequency could be used to vary the natural frequency of vibration of the actuation system and hence both variables could be used to in the control system of the actuator.

TABLE I PZT-S42 PIEZO-CERAMIC MATERIAL, TITANIUM SOLID RODS MATERIAL, AND THE STEEL BALL MATERIAL USED IN THE PROPOSED USM

Material	Coefficient (Unit)	Value
PZT-S42	Relative permittivity (Ωm)	1450
	Dissipation Constant (%)	0.4
	Mechanical Quality factor	600
	Density (g/cm^3)	7.6
Titanium Rod	Poisson's ratio	0.32
	Young`s Modulus of elasticity (Gpa)	116
	Density (g/cm^3)	16.69
steel Ball	Poisson's ratio	0.3
	Young`s Modulus of elasticity (Gpa)	70
	Density (g/cm^3)	2.7

TABLE II TRANSFORMATION OF E-COEFFICIENT TO D-COEFFICIENT FOR PIEZOCERAMIC MATERIAL USED IN USM MODELLING

Material	Coefficient	Value (m/v)
Piezo-ceramics	D_{31} x 10^{-12}	-155
	D_{33} x 10^{-12}	320

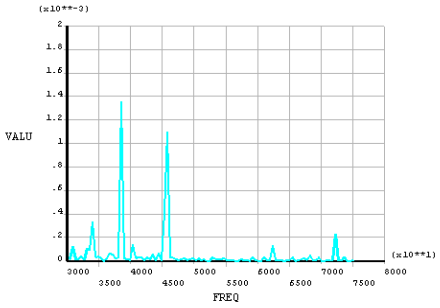

Figure 8 The variations of the PZT vibration ring displacement vs. frequency at 40 volt of the proposed USM actuator using single flexural vibration transducer

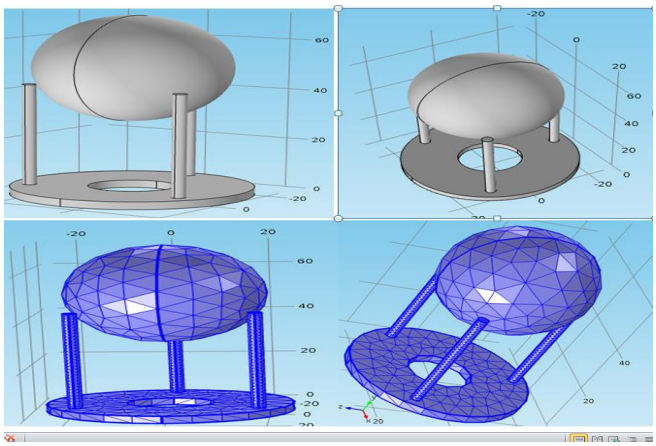

Figure 9 FEA model at drawn frequency of 39.709 kHz of the proposed USM actuator using single flexural vibration transducer

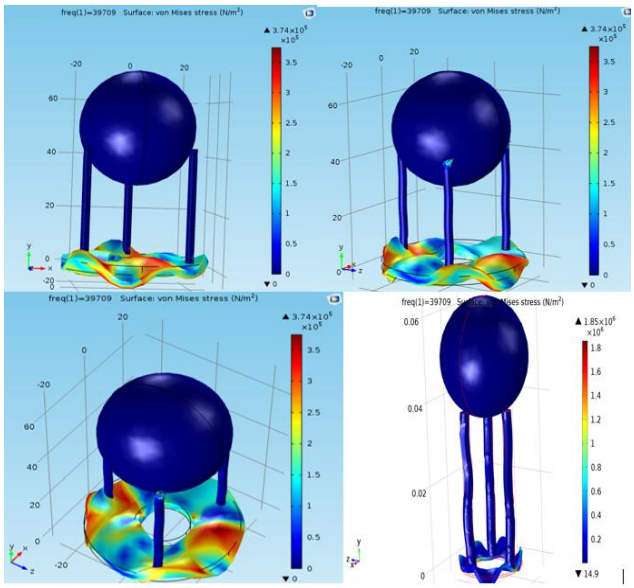

Figure 10 FEA model at drawn frequency of 39.709 kHz of the proposed 3D USM actuator using single flexural vibration transducer

The natural frequency of the actuator stator indicates the dynamic time response of the USM and in this case it is on the order of microseconds. This can be calculated roughly as Q times the vibration period. Where Q is the quality factor of the actuator, which can be determined using the following relationship [17-18]:

$$Q = \frac{R_m}{\sqrt{\frac{L}{C_\Sigma}}}$$

where R_m is the equivalent resistor of the vibrating transducer, at a fixed operating frequency, L is the inductance of the LC-driving circuit and C_Σ is the total capacitance which is not constant and depends on the vibrating transducer internal capacitance, cable internal capacitance and LC-driving circuit capacitance. **Figures 9** and **10** show the 3D USM FEA model at drawn frequency of 39.709 kHz for bending & longitudinal vibration mode. It shows also the material deformation, actuator structure and intersection between the actuator parts.

The FEA simulation and modelling enabled to test actuator structure, investigate material modes of vibration, material deformation, and select the PZT material of the flexural transducer ring, defining the operating parameters for the actuator, determining the principles of motion and possible technique to control the trajectory of motions, by controlling the phase between the modes of vibrations.

A prototype of the USM actuator was fabricated. The elements of the manufactured prototype were integrated successfully into the housing of the actuator and a series of experimental tests and measurements were carried out, to examine the potential characteristics of the developed prototype. **Figure 11** shows the fabricated prototype and **Figure 12** shows the arrangement used for testing. The

arrangement shown in **Figure 13** has been used to test and measure the actuator main characteristics. A piezoelectric driver was used to provide the Piezo-ceramic vibrating transducer ring with the alternative driving voltage and current. A function generator was used to provide various shapes of signal including sinusoidal, saw-tooth and square wave. A display unit, which consists of a digital oscilloscope and PC computer, was used to trace the signal and determine the actuator operating parameters.

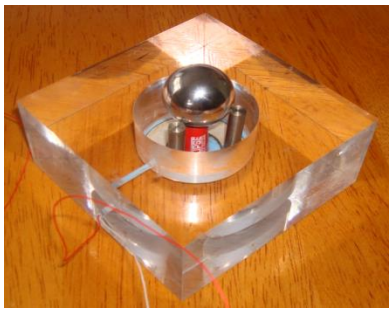

Figure 11 Fabricated prototype of the proposed USM using a single piezo-ceramic flexural vibrating ring transducer

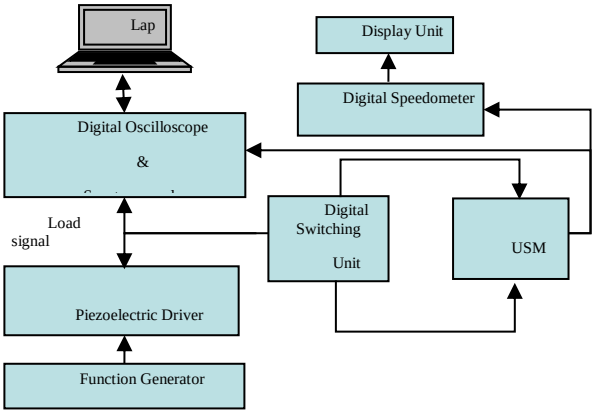

Figure 12 Block diagram of the arrangement used to measure characteristics of the fabricated USM prototype using single vibration ring

Figure 13 Practical test rig arrangement used to measure the characteristics of the fabricated USM actuator prototype using single flexural vibration transducer

A measurement of the operating parameters is carried out using the same arrangement used in the modelling of the actuator, as shown in Figures 2 and 7. The PZT ring transducer is connected to a single phase AC power source with a wide range of amplitude and frequency. A switching unit has been used to regulate the AC input power to the PZT ring transducer. Then a measurement of both the amplitude and frequency of the AC input signal is carried out. A sine wave input signal is obtained from a signal generator with the frequency sited to 100 kHz range. The input signal is monitored using the digital oscilloscope and the current is monitored using a digital Multi-meter. A gain of-25-amplification factor was obtained by changing the load range of the piezo driver model 603. The high voltage output is connected to the positive side of the piezoelectric ring and the ground of the piezo driver is connected to the negative one. The input signal from the signal generator is monitored on the oscilloscope. Voltage ranges of 1V -5V are selected. The voltage was increased in 1Volt intervals by adjusting the amplitude of the signal generator. The frequency of the input signal is adjusted on the signal generator, by gradually increasing it in 3-5 kHz intervals. The voltage and frequency is sequentially increased until the resonance frequency of the piezoelectric ring transducer is reached. The voltage is kept constant, and the frequency is adjusted until a trajectory is obtained. The trajectory is controlled by varying the frequency on the signal generator until a 3D rotational motion is obtained.

The frequency fixed at 39.53 KHz and the input voltage increased in sequential steps until reached 45Volt that when the rotor start move. The current and movement has been measured in revolution per minute (rpm) and the voltage has been recorded. **Figure 14** shows the variation of the current vs. input voltage for the fabricated USM prototype. This shows that the actuator is a capacitive load and the relationship graph can be used to determine its actuator internal impedance.

A constant voltage has been chosen of 100VAC, varying the frequency up and down between 38 kHz to 42 kHz, the movement trajectory of the rotor was moving in 3D. The frequency of USM driver has been altered incrementally. The speed of the actuator has been measured for each increment. It was noticed during this process that the speed of the actuator increases as the frequency of the actuator driver increased as shown in **Figure 15**. These measurements show the potential of using the voltage and or the frequency to control the 3D motions of the developed actuator. These measurements shows that the overall power consumption is in order of 5-watts. The resolution of the actuator was also measured and this found less than 5 micrometer.

A constant frequency has been chosen of 39.2 kHz, the voltage of USM driver has been altered incrementally. The speed of the actuator has been measured for each increment. **Figure 16** shows the relationship between the input voltage and the speed on rpm.

For autonomous vehicle and machine vision industrial applications, there is no much load will be carried out by the actuator. The maximum load that could be expected is the load of lenses and any other wireless sensors that could be integrated into the rotor. Therefore, the maximum load that the developed actuator can carry out was measured. This shows that the maximum load the prototype can carry out is equal to

3.5-Newton. **Figure 17** shows the variations of the speed of movement against the increase of the load attached incrementally to the sphere.

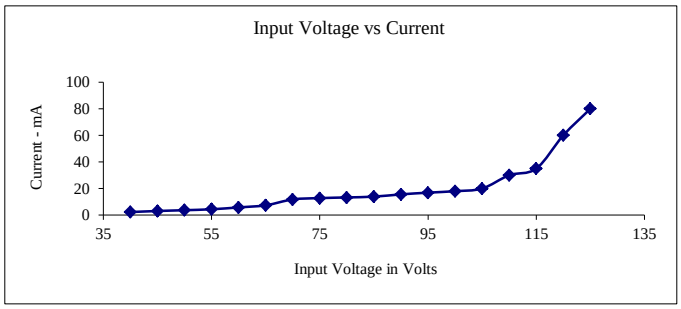

Figure 14 The variation of the current vs. input voltage for the fabricated 3D USM prototype using single flexural vibration transducer

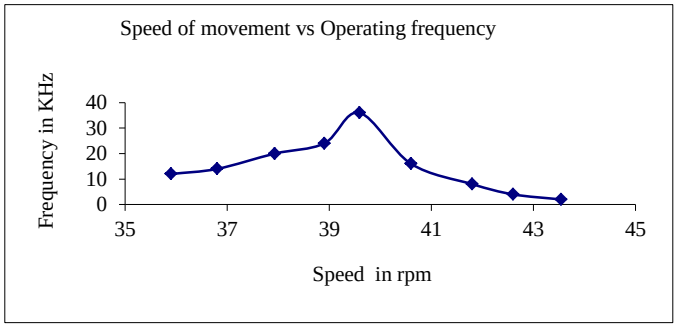

Figure 15 The variation of the speed of movement vs. the applied frequency for the fabricated 3D USM

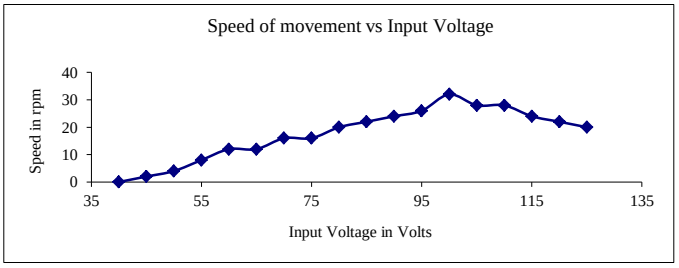

Figure 16 The variation of the 3D movement speed vs. input voltage for the fabricated 3D USM prototype using single flexural vibration transducer

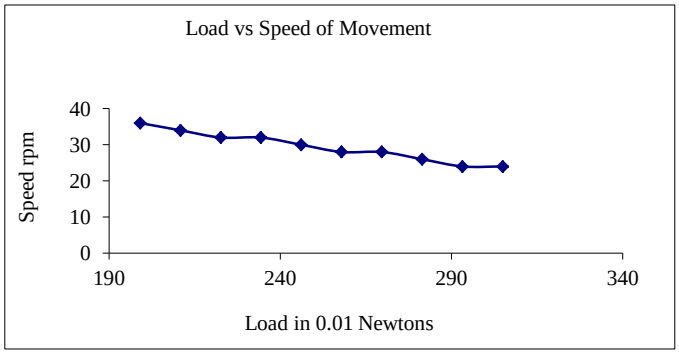

Figure 17 The variation of the speed of movement vs. load for the fabricated 3D USM prototype

The power was calculated as the operating parameters were found. Current is equal to 50 mA and voltage is equal to 100 volt. This shows that the overall power to drive such USM is low. The resolution of the rotor was measured and was found less than 5 micrometers, at nominal operating parameters of voltage of 100VAC, current of 50 mA and frequency of 39.53 KHz.

V. CONCLUSIONS

The development of a smart actuator with multidegree of freedom for autonomous vehicle industrial application have been developed and presented in this paper. The development life cycle of this actuator has passed through a number of stages. Finite element analysis has been utilised during the design process and has helped in design structure optimisation.

A prototype of the actuator fabricated and its characteristics were measured. Comprehensive experimental tests showed the ability of the developed actuator to provide 3D motions with multidegree of freedom, typical operating parameters are: frequency: 39.2 KHz, voltage: 100 volt and current: 50 m-amperes. This has indicated a close agreement with FEA results. The developed prototype has a speed of movement equal to 35 rpm, and a resolution of less than 5μm. It can also handle maximum load of 3.5-Newton.

These results shows the potential of the developed actuator to meet the essential requirements for machine vision digital visual data capture transducer for autonomous vehicle industrial application and could potentially increase the visual spotlight angle of digital visual data capture transducer.

It has been observed that there are few teething issues relevant to actuator motion trajectory and control algorithm. Research is still ongoing to tackle these issues and optimise the actuation system final design.

REFERENCES

[1] Ramesh Jain, Rangachar Kasturi, Brian G. Schunck, Machine Vision, McGraw-Hill, Inc., ISBN 0-07-032018-7, 1995.

[2] H. Golnabi, A. Asadpour, 'Design and application of industrial machine vision systems', Robotics and Computer-Integrated Manufacturing 23 (2007) 630–637. CrossRef

[3] Dimitris Gorpas, Kostas Politopoulos, Dido Yova, 'A binocular machine vision system for three-dimensional surface measurement of small objects', Computerized Medical Imaging and Graphics 31 (2007) 625–637. CrossRef

[4] SICK IVP, Machine Vision Introduction, Version 2.2, December 2006. VIEW

[5] Chunsheng Zhao, Ultrasonic motors: technologies and applications, Science Press, New York, 2011. CrossRef

[6] S. Lin, "An improved cymbal transducer with combined piezoelectric ceramic ring and metal ring", Elservier, China, sensors and actuators A: Physical Vol: 16 p-226-276, 2010.

[7] D. Engleke, B. Oehme, and J. Strackeljan, A Novel Drive Option for Piezoelectric Ultrasonic Transducers, Hindawi Publishing Corp, Modelling and Simulation in Engineering, Vol 2011, ID 910876, p1-6, 2011.

[8] J.S. Park, S.T. Kim, J.W. Kim, Ultrasonic linear motor using L1-B4 mode and its analysis, *Jpn. J. Appl. Phys.* 44 (1A) 412–416, 2005. CrossRef

[9] Yu. G. Martynenko, I.V. Merkuryev, and V.V. Podalkov. Control of Nonlinear Vibrations of Vibrating Ring Microgyroscope. *Mechanics of Solids*. Vol.43, No. 3, p379-390, 2008. CrossRef

[10] J. Jiamei, and Z. Chunsheng, A novel Traveling Wave Ultrasonic Motor Using a Bar Shaped Transducer, J.Wuham University of Technology, 2008.

[11] C.H. Yun, T. Ishii, K. Nakamura, S. Ueha, K. Akashi, A high power ultrasonic linear motor using a longitudinal and bending hybrid bolt-clamped Langevin type transducer, *Jpn. J. Appl. Phys*. 40 3773–3776, 2001. CrossRef

[12] F. Zhang, W.S. Chen, J.K. Liu, Z.S. Wang, Bidirectional linear ultrasonic motor using longitudinal vibrating transducers, *IEEE Trans. Ultrason. Ferroelectr. Freq. Control.* 52 (1) 134–138, 2005. CrossRef

[13] S.J. Shi, W.S. Chen, A bidirectional standing wave ultrasonic linear motor based on Langevin bending transducer, *Ferroelectronics* 350 102–110, 2008.

[14] M. Shafik, J. A. G. Knight, H. Abdalla, (2001), "Development of a new generation of electrical discharge texturing system using an ultrasonic motor", *13th International Symposium for Electromachining, ISEM, Spain*, May 9th to 11th, , 2001.

[15] M. Shafik, J. A. G. Knight, H Abdalla, "An investigation into electro discharge machining system applications using an ultrasonic motor", *Proceeding of ESM'-2002 International Conference, Belfast*, August 28th to 31st, 2002.

[16] M. Shafik & J. A. G. Knight, "Computer simulation and modelling of an ultrasonic motor using a single flexural vibrating bar", *Proceeding of ESM'2002 International Conference, Germany*, June 3rd to 5th, 2002.

[17] M. Shafik, 'Computer Aided Analysis and Design of a New Servo Control Feed Drive for EDM using Piezoelectric USM', PhD Thesis, De Montfort University, Leicester, UK, 2003.

[18] M. Shafik, E. M. Shehab and H. S. Abdalla, 'A Linear Piezoelectric Ultrasonic Motor Using a Single Flexural Vibrating Transducer for Electro Discharge System Industrial Applications', *Int. J. Adv. Manuf. Technol.* 45:287–299, 2009. CrossRef

[19] M. Shafik & S. Fekkai, (2012), 'A 3D Smart Actuator for Robotic Eyes Industrial Applications Using a Flexural Vibration Ring Transducer', 2012 International Conference on Innovations in Engineering and Technology for Sustainable Development (IETSD), India, 3-5 September, 2012.

[20] M. Shafik, et al, (2012), "Computer Simulation and Modelling of Standing Wave Piezoelectric Ultrasonic Motor Using Flexural Transducer, ASME 2012 International Mechanical Engineering Congress and Exposition, Houston, TX, USA.

[21] M. Shafik, et al, (2012), "Computer Simulation and Modelling of 3D Travelling Wave Piezoelectric Ultrasonic Motor Using a Flexural Vibration Ring Transducer, 2012 International Conference on Mechatronics and Computational Mechanics, Dubai, December 20 – 21, 2012.

[22] M. Shafik, et al, (2012), "Computer Simulation and Modelling of Standing Wave Piezoelectric Ultrasonic Motor Using a Single Flexural Vibration Transducer', 2012 International Conference on Mechatronics and Computational Mechanics, Dubai, December 20 – 21, 2012.

[23] He SY et al. "Standing wave bi-directional linearly moving ultrasonic motor", *IEEE trans. On Ultrasonics ferr. and freq. Control*, vol. 45, no. 5, 1998.

[24] J. Satonobu, and J. R. Friend. Travelling Wave Excitation in a Flexural Vibration Ring by Using a Torsional-Flexural Composite Transducer, IEEE Tran on Ultrasonics, Ferroelectrics and Frequency Control, Vol. 48, No. 4, 2001.

[25] Tobias H., Jorg Wallaschek, "Survey of the present state of the art of piezoelectric linear motors", *Ultrasonics*, 38, 37-40, 2000. CrossRef

[26] Woo Seok Hwang and Hyun Chul Park. "Finite element modelling piezoelectric sensors and actuators", AIAAJ, Vol. 31, No. 5, 1993. CrossRef

[27] Yingxiang Liu, Weishan Chen, Junkao Liu, Shengjun Shi, 'A cylindrical standing wave ultrasonic motor using bending vibration transducer', *Ultrasonics* 51 527–531, 2011. CrossRef

[28] S. Ben-Yaakov, et al, "A resonant driver for a piezoelectric motor", *Power Conversion and intelligent Motor Conference*, June, pp. 173-178, 1999.

[29] Ueha S. and Tomikawa Y. "*Ultrasonic motors theory and applications*", Clarendon press, Oxford, London, UK, 1993.

[30] Jacob Tal., "Servomotors take piezoceramic transducers for a ride", Machine Design (ISSN 0024-9114), *Penton Media, Inc.*, USA, 1999.